

# Micromachined Patch Antennas

Ioannis Papapolymerou, *Student Member, IEEE*, Rhonda Franklin Drayton, *Member, IEEE*,  
and Linda P. B. Katehi, *Fellow, IEEE*

**Abstract**— This paper presents the use of selective lateral etching based on micromachining techniques to enhance the performance of rectangular microstrip patch antennas printed on high-index wafers such as silicon, GaAs, and InP. Micromachined patch antennas on Si substrates have shown superior performance over conventional designs where the bandwidth and the efficiency have increased by as much as 64% and 28%, respectively. In this work, the silicon material is removed laterally underneath the patch antenna to produce a cavity that consists of a mixture of air and substrate with equal or unequal thicknesses. Characterization of the micromachined patch antenna is presented herein and includes a discussion on the bandwidth improvements, radiation patterns, and efficiency of the patch. In addition, antenna placement on the reduced index cavity with respect to the high-index substrate is described to achieve efficiency improvements over conventional patch antennas.

**Index Terms**— Microstrip antennas.

## I. INTRODUCTION

MICROSTRIP antennas are used in a broad range of applications from communication systems (radars, telemetry, and navigation) to biomedical systems, primarily due to their simplicity, conformability, low manufacturing cost [1], and enormous availability of design and analysis software. As system requirements for faster data transmission in lighter compact designs drive the technology area, higher frequency design solutions with large density layouts require integration of microwave devices, circuitry, and radiating elements that offer light weight, small size, and optimum performance. Compact circuit designs are typically achieved in high-index materials, which is in direct contrast to the low-index substrates imposed by antenna performance requirements. The ideal solution requires the capability to integrate the planar antenna on electrically thick low-index regions while the circuitry remains on the high-index regions in the same substrate. In the past, this requirement was satisfied by selecting the substrate that offers optimum component performance; unfortunately this led to hybrid integration schemes and high development cost. As the frequency increases, however, this approach becomes increasingly difficult and costs are prohibitively high. Microstrip patch antennas printed on high-index substrates are revisited in this

Manuscript received August 1, 1996; revised October 21, 1997. This work was supported by the Office of Naval Research under Contract N00014-92-J-1070 and the Army Research Office (MURI Program) under Grant DAAL03-92-G0109.

I. Papapolymerou and L. P. B. Katehi are with the Electrical Engineering and Computer Science Department, Radiation Laboratory, University of Michigan, Ann Arbor, MI 48109 USA.

R. F. Drayton is with the Electrical Engineering and Computer Science Department, University of Illinois at Chicago, IL 60607 USA.

Publisher Item Identifier S 0018-926X(98)01497-5.

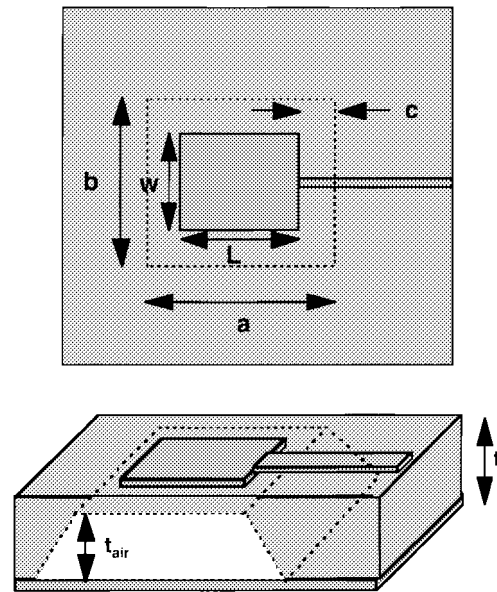


Fig. 1. Geometry of the micromachined patch antenna with mixed air-substrate region that has been laterally etched away.

work with the primary objective to develop design solutions that can be integrated into monolithic circuit layouts while enhancing antenna performance.

Microstrip antenna designs show significant performance degradation due to the pronounced excitation of surface waves in high-index materials. As a result, the antenna has lower efficiency, reduced bandwidth, degraded radiation patterns and undesired coupling between the various elements in array configurations. Optimum antenna performance depends on the choice of dielectric material as well as the choice of feeding network and is achieved when the radiated power occurs primarily as space waves with little or no components of “undesired” surface waves. Such microstrip designs are typically fabricated on electrically thick low-index materials and characterized by maximum antenna bandwidth and efficiency as reported by a vast number of theoretical and experimental researchers.

Only a few experimental approaches have been put forth to resolve the excitation of substrate modes in microstrip antennas. In 1984, a substrate–superstrate configuration [2] using a horizontal antenna element showed an increase in the radiation efficiency. Superstrate materials such as GaAs or Si, however, require a very thin substrate thickness that yields exceedingly small values of radiation resistance. In the past three years, researchers have begun to use physical substrate alterations as a means of perturbing the surface wave excitation. Circular patch designs in duroid [3] are based on

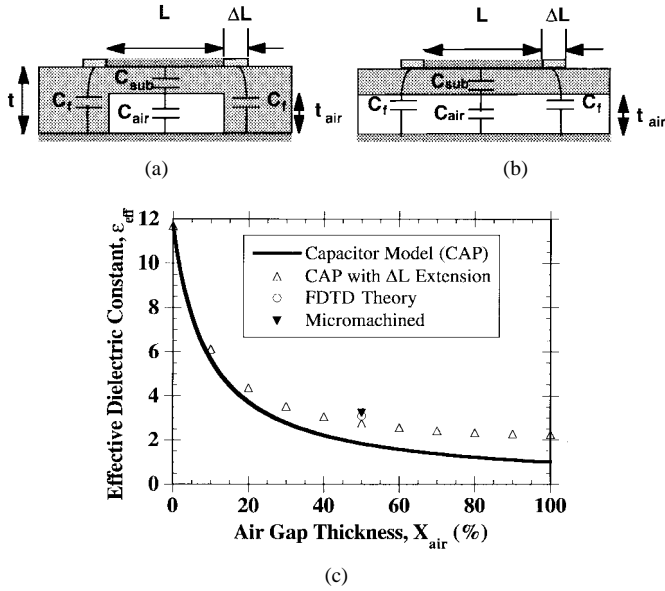


Fig. 2. Geometries used to determine the capacitance model for the micromachined patch antenna for (a) radiating edges into the high-index silicon substrate and (b) radiating edges over the mixed air-substrate cavity. (c) Graph of effective dielectric constant versus air gap thickness (percent) for the silicon based micromachined patch using the cavity and FDTD model compared to the measured response of the micromachined antenna [(a) geometry].

the choice of an appropriate patch radius to suppress the excited surface waves. Given the patch radius for a desired operating frequency, the antenna is forced to resonate at the first higher order mode ( $TM_{120}$ ) rather than the dominant ( $TM_{110}$ ) one. Other approaches rely on suspending the rectangular patch over an air cavity through the use of a membrane or over closely spaced periodic holes in the substrate (either drilled or micromachined) [4], [5]. In both cases, the radiation efficiency is increased and antenna patterns are improved considerably as a result of the elimination of surface wave propagation. Herein, an approach different from the ones described above is followed that does not require the use of holes or dielectric membranes [6]–[8]. In this study, material is removed underneath the antenna by using selective etching techniques and the excitation of surface waves is suppressed by creating a micromachined cavity (as shown in Fig. 1) that produces a low permittivity environment for the patch antenna.

The micromachined planar antenna design can be integrated on the same wafer with Si and GaAs IC's without affecting circuit requirements. In order to demonstrate the capability of a micromachined antenna to be integrated effectively with circuits, an example of a microstrip patch fed by a microstrip line is studied. More specifically, the antenna is printed on a cavity region that is comprised of two dielectric sections: 1) air and 2) silicon substrate. Using micromachining techniques, silicon is laterally removed from the cavity region producing a silicon area that has thickness less than or equal to 50% of the original substrate thickness and an air region that is created by the removal of material. Described herein is the characterization of a silicon micromachined patch antenna. In order to characterize the patch, a cavity model is used to estimate the reduced effective dielectric constant while bandwidth

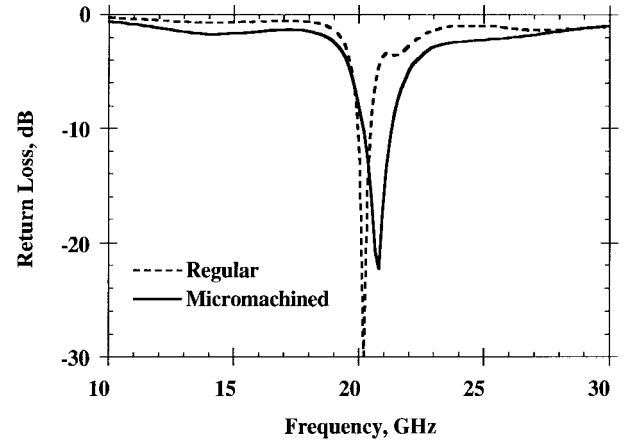


Fig. 3. Return loss measurement of the regular and micromachined patch antenna printed on a full thickness substrate and substrate with mixed air-silicon thickness ratio (1 : 1), respectively.

and radiation patterns are measured to evaluate the antenna's performance. Lastly, evaluation of the antenna's efficiency using available test equipment is achieved by fabricating and measuring a duroid-based scaled model.

## II. MICROMACHINED PATCH ANTENNA

To integrate patch antennas into circuit designs on high-index substrates without losing the advantages of low-index materials, the regions in the substrate, which will house the radiating elements must have low index of refraction. This is achieved by using micromachining to eliminate a portion of the substrate material (see Fig. 1). The micromachined antenna configuration consists of a rectangular patch centered over the cavity, sized according to the effective index of the cavity region, and fed by a microstrip line. To produce the mixed substrate region, silicon micromachining is used to laterally remove the material from underneath the specified cavity region resulting in two separate dielectric regions of air and silicon. In this work, the amount of silicon removed varies from 50 to 80% of the original substrate thickness underneath the patch and a cavity model is described in the next section to provide an estimate of the reduced index value. The walls of the hollowed cavity are in general slanted due to the anisotropic nature of the chemical etching. In Section II-B, the scattering parameter measurements illustrate the antenna's bandwidth, while field patterns indicate the radiated power.

### A. Calculation of Reduced Dielectric Constant

A cavity model is used to predict the effective dielectric constant of the mixed air-silicon region for varying thickness ratios underneath the patch antenna. A quasi-static model based on series capacitors is used to determine the patch capacitance in the mixed region [Fig. 2(a)]

$$C = \frac{\epsilon_{eff} A}{t} \quad (1)$$

where  $\epsilon_{eff} = \epsilon_{reff} \epsilon_0$ . For simplicity the walls of the cavity are assumed to be vertical and the effective dielectric constant

TABLE I  
DESIGN PARAMETERS FOR THE ANTENNAS ON SILICON SUBSTRATES

Patch	t (mm)	t <sub>air</sub> (mm)	L (mm)	w (mm)	a (mm)	b (mm)	c (mm)
Regular	0.355	0	2.019	4.08	0	0	0
Microma- chined	0.355	0.165	3.616	3.445	3.616	8.108	0

( $\epsilon_{\text{reff}}$ ) is estimated by the following expression:

$$\epsilon_{\text{reff}} = \epsilon_{\text{cavity}} \left( \frac{L + 2\Delta L \frac{\epsilon_{\text{fringe}}}{\epsilon_{\text{cavity}}}}{L + 2\Delta L} \right) \quad (2)$$

$$\frac{\epsilon_{\text{fringe}}}{\epsilon_{\text{cavity}}} = \frac{\epsilon_{\text{air}} + (\epsilon_{\text{sub}} - \epsilon_{\text{air}})x_{\text{air}}}{\epsilon_{\text{air}} + (\epsilon_{\text{sub}} - \epsilon_{\text{air}})x_{\text{fringe}}}$$

where

$$\epsilon_{\text{cavity}} = \frac{\epsilon_{\text{air}}\epsilon_{\text{sub}}}{\epsilon_{\text{air}} + (\epsilon_{\text{sub}} - \epsilon_{\text{air}})x_{\text{air}}} \quad (3)$$

In the above expressions,  $\epsilon_{\text{cavity}}$  represents the relative dielectric constant of the mixed substrate region and  $\epsilon_{\text{fringe}}$  represents the relative dielectric constant in the fringing fields region. Equation (2) includes the open-end effect extension length  $\Delta L$  to the antenna, which can be found from [9] where  $\epsilon_{\text{fringe}}$  is the permittivity used for the calculation of  $\Delta L$ . The thickness parameters  $x_{\text{air}}$  and  $x_{\text{fringe}}$  are ratios of the air to full substrate thickness in the mixed and fringing field regions, respectively. For the silicon micromachined case shown in Fig. 2(a)  $x_{\text{fringe}}$  is taken as zero, whereas for the case of Fig. 2(b)  $x_{\text{fringe}} = x_{\text{air}}$ .

A plot of the theoretical and measured effective dielectric constant versus the air gap thickness for silicon substrate ( $\epsilon_r = 11.7$ ) can be found in Fig. 2(c), where an effective dielectric constant of approximately 2.2 is achieved for a mixed air-silicon ratio of 1:1 using the capacitor model [(2) with  $\Delta L = 0$ ] and 3:1 ratio for the capacitor model with  $\Delta L$  extension length ((2) with  $\Delta L$  calculated from [9]). The dimensions for the micromachined patch that was used to produce the results of Fig. 2(c) can be found in Table I (parameters a, b, and c, are actual values since the walls are assumed vertical). Included also in Fig. 2(c) is a data point based on the finite difference time-domain model of the micromachined patch geometry. The finite-difference time-domain (FDTD) calculation was based on a three-dimensional (3-D) full-wave scheme that yields the return loss of the micromachined antenna and the effective permittivity of an 1:1 air-silicon substrate for a range of frequencies. Once the resonant frequency is determined from the return loss, the effective permittivity of interest is found. Only one case of air-silicon substrate ratio has been simulated with FDTD in order to validate the quasi-static results for the effective dielectric constant of the antenna that was fabricated and tested. Regarding the measured (“micromachined”) data point of Fig. 2(c), the resonant frequency of the fabricated antenna was measured and [10] was used to extract the dielectric constant of the substrate for a patch having the same dimensions as the measured one. In the following sections,

more extensive experimental data will be presented that prove the superiority of this type of micromachined antenna. The conventional and micromachined antennas will be defined as a patch fabricated on a regular substrate or as a patch fabricated on a substrate that has locally reduced index region, respectively.

### B. K-Band Micromachined Patch

Two antennas were fabricated on silicon, with resonant frequencies in the K-band and air/substrate thickness ratios of 1:1 (see Table I for dimensions). In the silicon micromachined patch (SMP) antenna, the conductor has been electroplated to a metal thickness of approximately  $3.2 \mu\text{m}$  and the substrate is chemically etched (EDP process) in a single-etch step underneath the antenna. Since the walls of the resulting cavity are not vertical due to the anisotropic etching, dimensions for a, b, and c in Table I represent average values. The lower ground plane is achieved by attaching adhesive copper tape of  $25.4 \mu\text{m}$  thickness and the size of the silicon substrate where the antennas were fabricated was approximately  $2.8 \times 3 \text{ cm}$ . Return loss measurements are shown in Fig. 3 and were obtained using an HP 8510 Network Analyzer where the bandwidth ( $|S_{11}| \leq -10 \text{ dB}$ ) increases from 2.9% for the “regular” antenna to 5% for the SMP. Since bandwidth is inversely proportional to the quality factor Q, defined as the ratio of total energy stored in the antenna to the energy dissipated or radiated from the antenna, the increase in bandwidth provides the first indicator of an increase in total radiation from the antenna. Efficiency measurements, however, need to be made in order to observe the increase in power radiated into space waves as opposed to power radiated into surface waves.

Radiation patterns were also taken for the two antennas and the results are shown in Fig. 4, where significant differences in the *E*-plane pattern are observed while the *H*-plane patterns remain similar as expected. For measurement purposes, the silicon substrates that hosted the antennas were mounted on a  $5.6 \times 5 \text{ cm}$  metallic holder that served as the ground plane. The silicon antenna pattern exhibits many ripples, that are due to the diffraction of strong surface waves from the edges of the finite ground plane. In contrast, the micromachined antenna pattern is much smoother. Conclusive evidence, needed to show the suppression of surface waves, is obtained by evaluating the antenna gain and measured efficiency. Since test equipment at this frequency was unavailable, a scaled model has been developed for designs printed on high-index (10.8) duroid substrate that operate at Ku-band resonant frequencies.

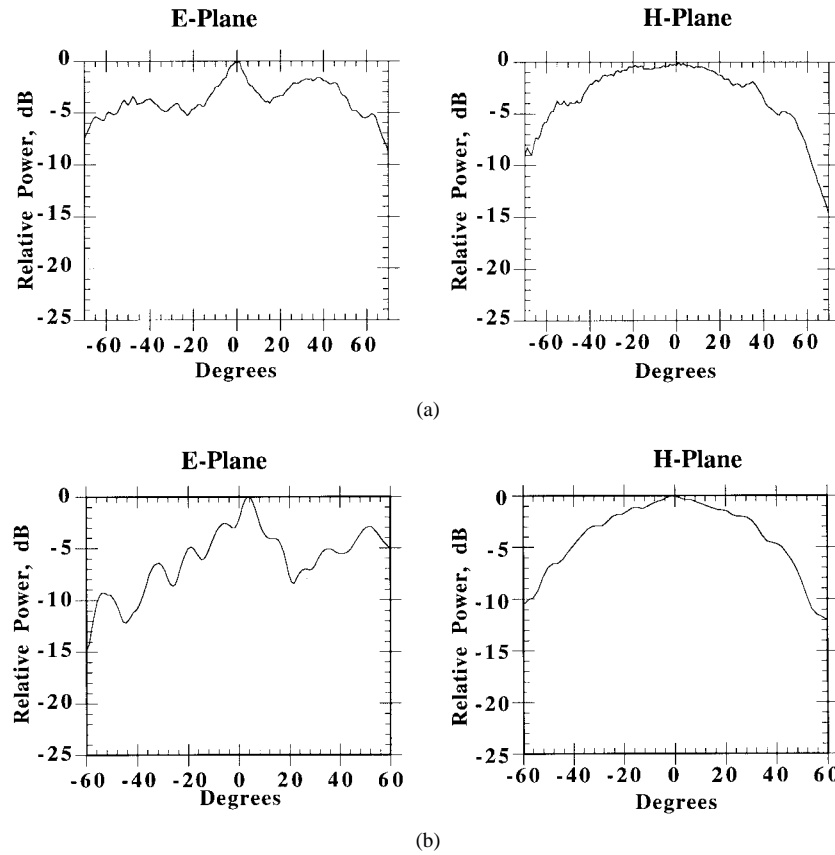


Fig. 4. *E*- and *H*-plane radiation patterns of the (a) micromachined antenna on silicon and of the (b) regular antenna on silicon.

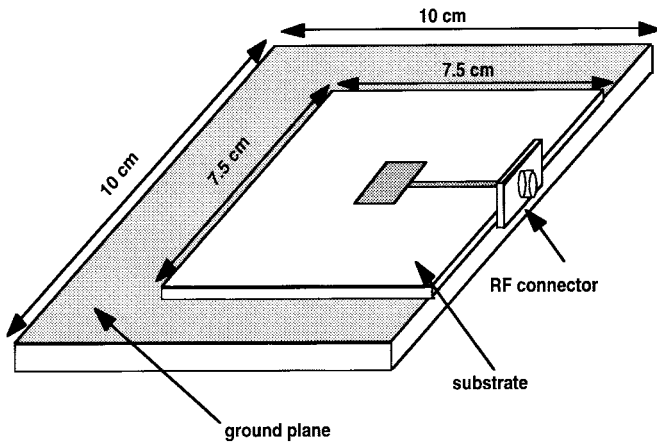


Fig. 5. Test fixture with micromachined antenna mounted.

### III. CHARACTERIZATION OF MICROMACHINED PATCH ANTENNAS

The last step in characterizing the micromachined patch performance is the evaluation of the antenna's efficiency. In order to utilize existing test equipment, a scaled model of the antenna is fabricated on a mixed air-substrate cavity and is realized by machining a high-index (10.8) duroid substrate. During this phase, a comparison is made between the micromachined patch and conventional designs operating at the same frequency. Similar measurements to those of the micromachined antennas are obtained to determine the bandwidth and radiation pattern of the scaled models in addition to the measured efficiency.

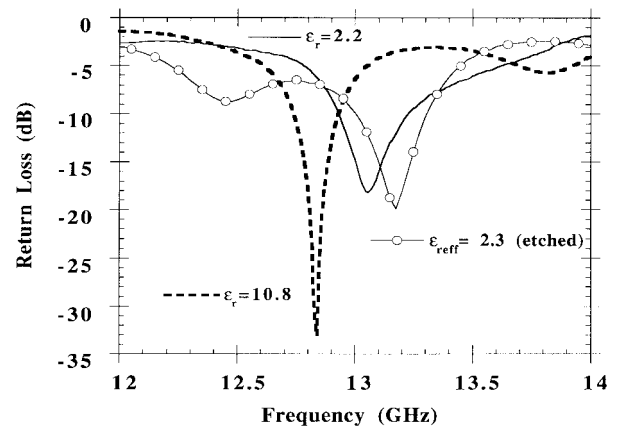


Fig. 6. Measured return loss for the scaled model patch antenna  $\epsilon_{\text{reff}} = 2.3$  (etched) and regular patch antennas  $\epsilon_r = 2.2$  and  $\epsilon_r = 10.8$ .

In the remaining sections, the theory of radiation-efficiency measurements is described first. Next, the antenna performance is characterized based on bandwidth, radiation patterns, and efficiency. Lastly, design parameters are discussed regarding the size of the micromachined cavity to produce enhanced efficiency over conventional designs.

#### A. Theory of Radiation Efficiency

To obtain the antenna gain of the patch antenna, radiation efficiency based on a radiometric method is used, which compares the noise power of a lossy antenna under test (AUT)

TABLE II  
DIMENSIONS OF THE FABRICATED SCALED MODEL AND REGULAR ANTENNAS

Patch	t (mm)	t <sub>air</sub> (mm)	L (mm)	w (mm)	a (mm)	b (mm)	c (mm)
Regular (10.8)	0.635	0	3.750	4.420	0	0	0
Scaled Model (10.8)	0.635	0.476 (75%)	7.624	6.676	15.190	14.478	3.783
Regular (2.2)	0.500	0	7.570	7.340	0	0	0

TABLE III  
INPUT IMPEDANCE CHARACTERISTICS OF THE REGULAR AND SCALED MODEL ANTENNAS

Patch	Input Impedance ( $\Omega$ )	Resonant Frequency (GHz)	Feed Line Length (mm)
Regular (10.8)	49.2 - j0.37	12.84	27.6
Scaled model (10.8)	67.5 - j1.04	13.165	27
Regular (2.2)	67.5 - j0.14	13.044	34

to a known load [11], [12]. Antenna efficiency is obtained by characterizing the system receiver and then the composite system (system receiver plus antenna). By measuring output powers of the receiver when connected to a hot ( $P_L^H$ ) or cold ( $P_L^C$ ) 50  $\Omega$  load, the noise factor is given in [13] as

$$F_r = \frac{(T_{HL} - T_{CL})}{T_{HL}(1 - 1/Y_r)} \quad (4)$$

where the measured power ratio  $Y_r$  is  $P_L^H/P_L^C$  and the temperatures are  $T_{HL} = 295$  K and  $T_{CL} = 77$  K for hot and cold load, respectively.

Individual AUT's are measured in the composite system to obtain hot and cold measurements where the black body absorber (Ecosorb), placed in front of the antenna element, has been held at room temperature ( $T_{HA} = 295$  K) for the hot load and has been immersed in liquid nitrogen ( $T_{CA} = 77$  K) for the cold load. Note that the 50- $\Omega$  calibration load is submersed into the liquid nitrogen. The resulting composite system noise factor is expressed as

$$F_C = \frac{(T_{HA} - T_{CA})}{T_{HA}(1 - 1/Y_C)} \quad (5)$$

where the measured power ratio of the antenna  $Y_C$  is  $P_A^H/P_A^C$ . Since the measured output noise powers of the receiver and the composite system with the hot load is known, the antenna gain can be obtained from the following expressions:

$$P_L^H = KT_{HL} BG_r F_r \quad (6)$$

$$P_A^H = KT_{HA} BG_r G_A F_C \quad (7)$$

where  $G_r$  and  $G_A$  are the receiver and antenna gain, respectively. After dividing the two hot-load power equations [(7) by (6)] and substituting in the noise factor parameters [ $F_r$  (4) and  $F_C$  (5)], the antenna gain expression becomes

$$G_A = \frac{P_A^H - P_C^H}{P_L^H - P_L^C} \quad (8)$$

Equation (8) assumes equal temperatures for the 50- $\Omega$  load and AUT in either the cold ( $T_{HL} = T_{HA} = 295$  K) or hot ( $T_{CL} = T_{CA} = 77$  K) load measurement.

A modified gain expression is shown in (9) that accounts for temperature differences observed in the application of the test methodology in the measurement of the cold 50- $\Omega$  load and AUT. Since the absorber is immersed into liquid nitrogen and then removed to cover the antenna, the cold temperature is slightly elevated and is taken as  $T_{CA} = 88$  K while the 50- $\Omega$  load, submersed continuously into the liquid nitrogen, maintains a constant temperature  $T_{CL}$  of 77 K. Hence,

$$G_A = 1.038 \frac{P_A^H - P_A^C}{P_L^H - P_L^C} \quad (9)$$

### B. Ku-Band Micromachined Patch Antenna

Since the available measurement setup imposes an operating frequency range between 12.5 and 13.5 GHz, several rectangular patch designs are fabricated on duroid substrates of high (10.8) and low (2.2) index constants with substrate thickness  $t$  of 635 and 500  $\mu$ 's, respectively. Scaled model micromachined antennas were also fabricated in which the cavity is created by machine milling. The final geometry is similar to those shown in Fig. 1 without the sloping sidewalls and the dimensions for the various antennas can be found in Table II, where the parameters  $a$  and  $b$  are given by their actual values and not the average ones since the sidewalls are vertical. To describe the findings of the various patch configurations investigated, the notation used in the following sections refers to antennas on full thickness substrates as "regular" high- (10.8) or low- (2.2) index designs and those printed on a mixed air-duroid cavity as scaled models. Each patch is fed by a 50- $\Omega$  microstrip feedline, is fabricated on a (75 mm)<sup>2</sup> substrate, and is mounted in the test fixture shown in Fig. 5. Since the micromachined scaled model antenna resides over the mixed dielectric material, approximately 3.65 mm of the feed line has an impedance

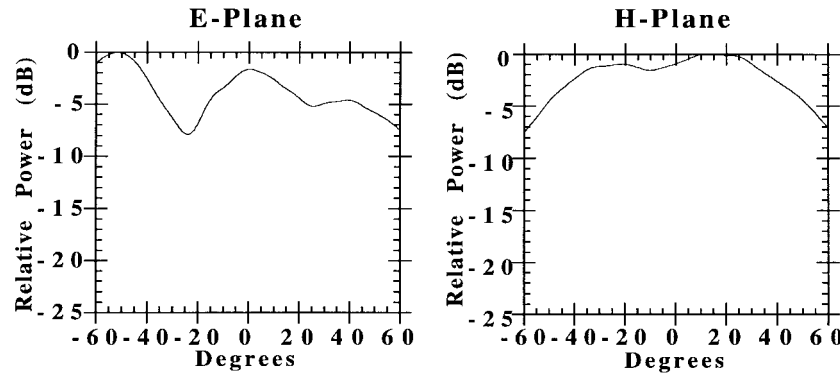


Fig. 7. Radiation patterns of a regular high-index patch antenna ( $\epsilon_r = 10.8$  and  $t = 635 \mu\text{m}$ ) at 12.84-GHz resonant frequency.

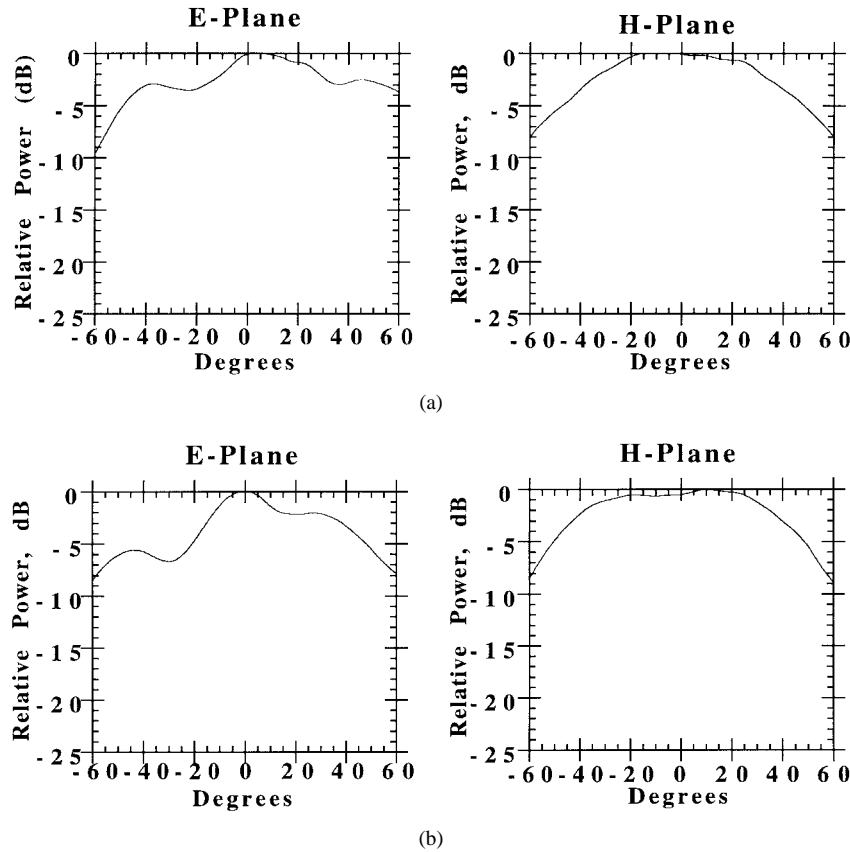


Fig. 8. *E*- and *H*-plane radiation patterns for (a) patch antenna on low-index duroid substrate ( $\epsilon_r = 2.2$  and  $t = 500 \mu\text{m}$ ) at resonant frequency of 13.044 GHz and (b) scaled model on a duroid substrate ( $\epsilon_r = 10.8$  and  $t = 635 \mu\text{m}$ ) at resonant frequency of 13.165 GHz.

based on the mixed air-duroid region compared to the feedline of regular antennas on full thickness material. The width of the feeding line ( $560 \mu\text{m}$ ) for the scaled model patch is maintained over the mixed region and is the same width of the  $50\text{-}\Omega$  line on full substrate resulting in a characteristic impedance of approximately  $96 \Omega$ . The return loss is measured (Fig. 6) and the input impedance values referenced at the RF connector are shown in Table III; notice the good agreement between the scaled model and regular low-index antenna. In Fig. 6 the bandwidth of the scaled model increases to 2.3%, a 100% increase over the  $-10\text{-dB}$  bandwidth of the regular patch printed on the high-index material. This increase in bandwidth is also observed in the silicon micromachined antenna and is

an indication of the expected increase in total power (space and surface waves) radiated from the patch.

To minimize the interaction between the connector and the antenna in the radiation pattern measurements, a small piece of absorber is placed over the RF connector to reduce the effects of secondary reflections on the antenna pattern. In Fig. 7 the “regular” high-index pattern has a large peak in the *E* plane at approximately  $-50^\circ$ , indicating large power leakage to surface waves. This behavior is also observed in [4]. In contrast, the scaled model patch shown in Fig. 8 has a much smoother *E*-plane pattern and is very similar to the *E*-plane pattern of the “regular” low-index antenna. As expected, the *H*-plane patterns are similar in all cases. The difference between the *E*-

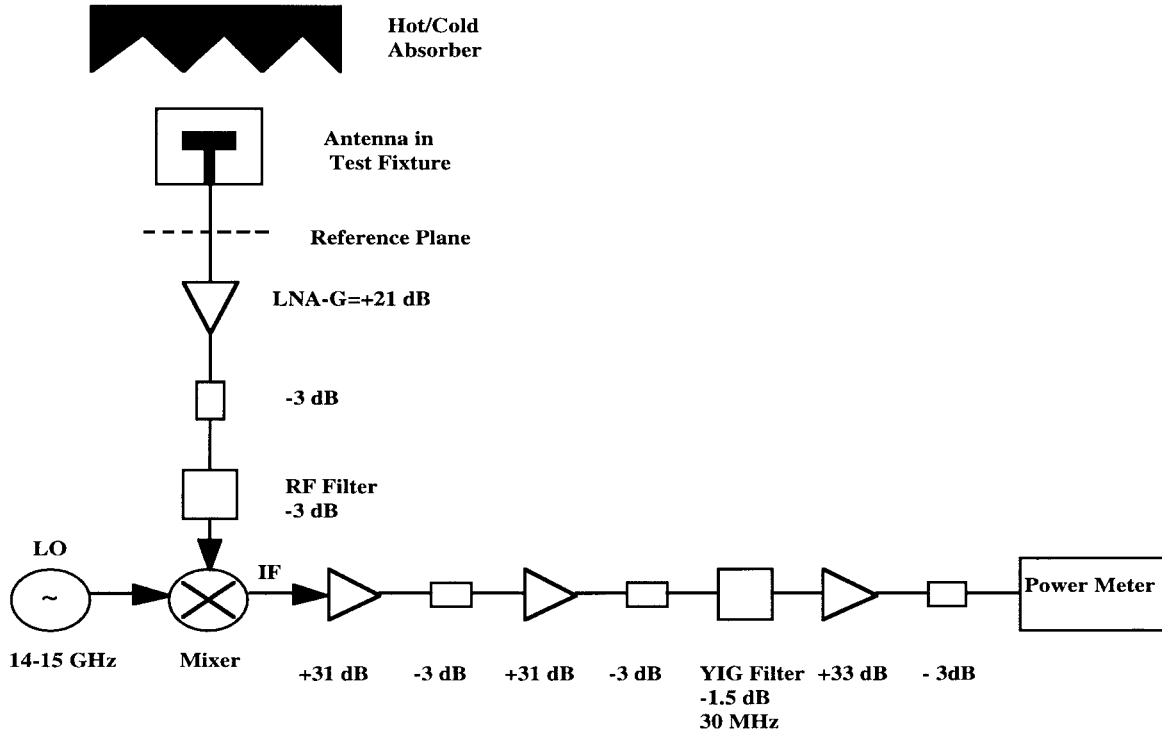


Fig. 9. System diagram of the efficiency measurement setup.

plane patterns of Figs. 4(b) and 7 (both antennas are “regular”) can be attributed to the slightly different dielectric constant, the different experimental setup used for the pattern measurements and the fact that the distance between the antenna and the edge of the finite ground plane is not the same in terms of guided wavelengths.

### C. Efficiency Measurements

The system configuration [5] is illustrated in Fig. 9 and has component specifications consisting of an RF bandpass filter with an insertion loss of 3 dB in the 12.5–13.5 GHz range and a mixer intermediate frequency (IF) of 1.5 GHz. Since the calibration plane of the system is at the RF connector, the measured efficiency values include the feed line, connector and mismatch losses. In order to determine the de-embedded antenna efficiency, the losses must be determined and extracted. The losses associated with the feed line lengths (Table III) are calculated using HP Momentum [5], [14], the RF connector loss is based on an empirical value, and the mismatch loss is determined from the measured return loss data.

In Fig. 10, the measured efficiency data, which are averaged values, show  $73 \pm 3\%$  for the scaled model having an air-substrate thickness ratio of 3:1 and  $56 \pm 3\%$  for the “regular” antenna printed on the high-index material. The patch printed on 2.2 duroid was found to have an efficiency of  $76 \pm 3\%$ . In Table IV, a summary of the measured efficiency, specific losses, and de-embedded efficiency are documented. The scaled model case shows sensitivity to the distance  $c$  between the radiating edges of the antenna and the edges of the micromachined cavity. From the results summarized in Table V, it can be observed that for an air-substrate thickness ratio of 1:1 and separation  $c = 0$ , the efficiency of the

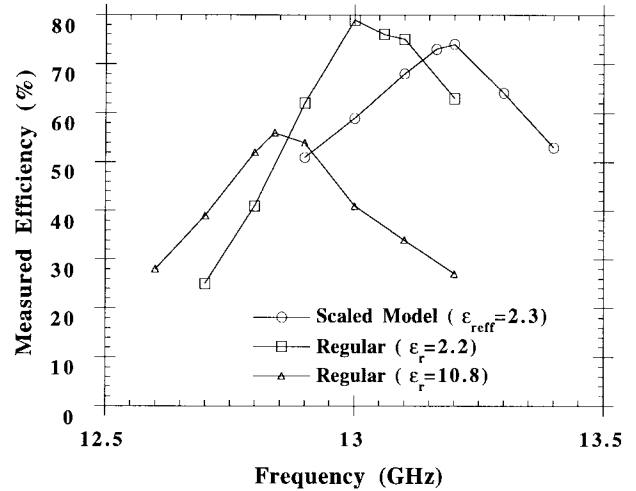


Fig. 10. Measured efficiency for the scaled model and regular patch antenna designs.

scaled model is similar to that of a patch on high-index substrate. However, when the distance is at least twice the substrate thickness  $2t$  for the same air-substrate thickness ratio, the de-embedded efficiency increases by about 10%. This is further validated in the measured data shown in Table IV for a distance of  $c = 3.783$  mm (six times the substrate height  $6t$ ). The improvements observed are attributed to the presence of fringing fields that usually extend one to two times the thickness  $t$  beyond the radiating edges of the antenna into the substrate environment. The above results emphasize the importance of the air-substrate thickness ratio on bandwidth and also the importance of the distance between the radiating edge of the antenna and the micromachined cavity in order to enhance the antenna’s efficiency.

TABLE IV  
DE-EMBEDDED EFFICIENCY FOR THE SCALED MODEL AND REGULAR PATCH ANTENNAS AT RESONANCE

Antenna	Regular $\epsilon_r=10.8$	Scaled Model $\epsilon_r=10.8$	Regular $\epsilon_r=2.2$
<b>Measured Efficiency</b>			
Based on Equation (8)	56%	73%	76%
Based on Equation (9)	58%	76%	79%
Mismatch loss (dB)	0 (100%)	0.05 (99%)	0.08 (98%)
Connector loss (dB)	0.15 (97%)	0.15 (97%)	0.15 (97%)
Feed line loss (dB)	0.56 (88%)	0.48 (90%)	0.1 (98%)
<b>Total loss (dB)</b>	0.71 (85%)	0.68 (86%)	0.33 (93%)
<b>De-embedded Efficiency</b>			
Based on Equation (8)	66%	85%	82%
Based on Equation (9)	68%	88%	85%

TABLE V  
EFFICIENCY RESULTS AND DIMENSIONS FOR TWO SCALED MODEL ANTENNAS ON DUROID SUBSTRATE WITH  $\epsilon_r = 10.8$

Patch Antenna	Mixed air-substrate thickness ratio (1:1) $c=0$	Mixed air-substrate thickness ratio (1:1) $c \approx 2t$
t (mm)	0.635	0.635
$t_{\text{air}}$ (mm)	0.330	0.330
L (mm)	5.415	7.624
w (mm)	6.676	6.676
a (mm)	5.415	10
b (mm)	10.590	14
Measured efficiency	52%	65%
Total loss (dB)	0.69 (85%)	0.69 (85%)
De-embedded efficiency	61%	76%

The de-embedded efficiencies of the individual antenna elements (see Table IV) are 85% for the micromachined scaled model and 66% and 82% for the antennas on 10.8 and 2.2 duroid substrate, respectively. As a result, the efficiency of the micromachined patch increases by 28% over the high-index patch and the efficiency performance approaches the patch on low-index duroid within the bounds of measurement error. When the modified efficiency expression is used to account for differences in the cold measurement of the  $50 \Omega$  load and AUT, the measured and de-embedded efficiencies increase by 2–3% as seen in Table IV. In this case, no significant difference is observed between either approach since the accuracy of the measurement system is 3%.

#### IV. CONCLUSIONS

The approach presented herein uses silicon micromachining techniques to physically alter the air-silicon thickness ratio by laterally removing material in selective regions of a high-index substrate. To meet design space constraints and

antenna performance requirements (bandwidth and radiation efficiency), this approach offers an easy method to optimize antenna size and maximize antenna performance in selective regions of circuits designed on high-index substrates. The overall dimensions of the radiating element are determined by the effective dielectric constant (or index) of the material and can range from its smallest size in a high-index material such as silicon ( $\epsilon_r = 11.7$ ) to its largest size in an air substrate ( $\epsilon_r = 1.0$ ) region.<sup>1</sup>

Characterization of the micromachined patch antenna has been presented to illustrate the advantages of selectively reducing the dielectric constant in specific locations of a high-index material in order to enhance patch antenna performance. Both antenna configurations show an increase in the impedance bandwidth and smoother  $E$ -plane radiation patterns compared to patch designs in high-index materials. Antenna efficiency measurements were performed on the scaled model reflecting

<sup>1</sup>A dielectric membrane supports the antenna element over an air cavity formed by etching the silicon entirely away.



similar values to the low-index patch antenna ( $\epsilon_r = 2.2$ ). For micromachined antennas, it is also shown that placement of the antenna's radiating edges with respect to the high-index region is critical to improving the power radiated as space waves and must be at least twice the substrate thickness. Finally, a comparison between the high-index patch and the micromachined scaled model shows bandwidth improvements by 64% from values of 1.4–2.3% and efficiency improvements by 28% from values of 66–85%, respectively. Therefore, enhanced antenna performance has been achieved using this micromachining approach where the bandwidth and efficiency improvements indicate that patch elements can be integrated in compact monolithic microwave integrated circuit (MMIC) designs on high-index environments.

#### ACKNOWLEDGMENT

The authors would like to thank Dr. G. Rebeiz and T. Ellis for assistance in fabricating the duroid-based antennas, G. Gauthier for helping with efficiency measurements, and Rogers Corporation, Chandler, AZ, for the generous donation of the duroid substrates. The assistance of Dr. R. Simons and Dr. R. Lee at NASA Lewis Research Center, Cleveland, OH, is also greatly appreciated in obtaining antenna pattern measurements.

#### REFERENCES

- [1] D. M. Pozar, "Microstrip antennas," *Proc. IEEE*, vol. 80, pp. 79–91, Jan. 1992.
- [2] N. G. Alexopoulos and D. R. Jackson, "Fundamental superstrate (cover) effects on printed circuit antennas," *IEEE Trans. Antenna Propagat.*, vol. AP-32, pp. 807–816, Aug. 1984.
- [3] D. R. Jackson, J. T. Williams, A. K. Bhattacharyya, R. L. Smith, S. J. Buchheit, and S. A. Long, "Microstrip patch designs that do not excite surface waves," *IEEE Trans. Antennas Propagat.*, vol. 41, pp. 1026–1037, Aug. 1993.
- [4] M. J. Vaughn, K. Hur, and R. C. Compton, "Improvement of microstrip patch antenna radiation patterns," *IEEE Trans. Antennas Propagat.*, vol. 42, pp. 882–885, June 1994.
- [5] G. P. Gauthier, A. Courtay, and G. M. Rebeiz, "Microstrip antennas on synthesized low dielectric-constant substrates," *IEEE Trans. Antennas Propagat.*, vol. 45, pp. 1310–1314, Aug. 1997.
- [6] T. M. Weller, L. P. B. Katehi, and G. M. Rebeiz, "High performance microshield line components," *IEEE Trans. Microwave Theory Tech.*, vol. 43, pp. 534–543, Mar. 1995.
- [7] R. F. Drayton and L. P. B. Katehi, "Development of self-package high frequency circuits using micromachining techniques," *IEEE Trans. Microwave Theory Tech.*, vol. 43, pp. 2073–2080, Sept. 1995.
- [8] S. V. Robertson, L. P. B. Katehi, and G. M. Rebeiz, "Micromachined W-band filters," *IEEE Trans. Microwave Theory Tech.*, vol. 44, pp. 598–606, Apr. 1996.
- [9] E. O. Hammerstad and F. Bekkadal, "A microstrip handbook," Univ. Trondheim, Norway, ELAB Rep., STF 44 A74169, N7034, 1975.
- [10] D. M. Pozar, *PCAAD: Personal Computer Aided Antenna Design*, Version 2.1, Dec. 1991.
- [11] J. Ashkenazy, E. Levine, and D. Treves, "Radiometric measurement of antenna efficiency," *Electron. Lett.*, vol. 21, no. 3, Jan. 1985.
- [12] D. M. Pozar and B. Kaufman, "Comparison of three methods for the measurement of printed antenna efficiency," *IEEE Trans. Antennas Propagat.*, vol. 36, no. 1, pp. 136–139, Jan. 1988.
- [13] D. M. Pozar, *Microwave Engineering*. Reading, MA: Addison-Wesley, 1993.
- [14] HP EEsof, Inc., Westlake Village, CA.



**Ioannis Papapolymerou** (S'90) received the B.S.E.E. degree from the National Technical University, Athens, Greece, in 1993, and the M.S.E.E degree from the University of Michigan, Ann Arbor, in 1994. He is currently working toward the Ph.D. degree in electrical engineering at the University of Michigan.

His research interests include the implementation of micromachining techniques in microwave and millimeter-wave circuits, the development of both passive and active planar circuits on silicon and GaAs for high-frequency applications, as well as numerical techniques for the characterization of those circuits.

Mr. Papapolymerou received the Outstanding Graduate Student Instructional Assistant Award in 1997 by the American Society for Engineering Education (ASEE), University of Michigan chapter.



**Rhonda Franklin Drayton** (S'85–M'95) received the B.S.E.E. degree from Texas A&M University, College Station, in 1988, and the M.S.E.E. and Ph.D. degrees from the University of Michigan, Ann Arbor, in 1990 and 1995, respectively.

She is currently an Assistant Professor in the Electrical Engineering and Computer Science Department at the University of Illinois, Chicago. Her current research interests include development of high-frequency planar circuits, antennas, and packages for microwave and millimeter-wave applications using micromachining techniques.

She received the Best Student Paper Award at the 1994 IEEE MTT-S International Microwave Symposium and the 1997 Amoco Silver Circle Award for Teaching Excellence from the University of Illinois at Chicago.



**Linda P. B. Katehi** (S'81–M'84–SM'89–F'95) received the B.S.E.E. degree from the National Technical University of Athens, Greece, in 1977, and the M.S.E.E. and Ph.D. degrees from the University of California, Los Angeles, in 1981 and 1984, respectively.

In September 1984, she joined the faculty of the Electrical Engineering and Computer Science Department of the University of Michigan, Ann Arbor. Since then, she has been interested in the development and characterization (theoretical and experimental) of microwave and millimeter-wave printed circuits, the computer-aided design of VLSI interconnects, the development and characterization of micromachined circuits for millimeter-wave and submillimeter-wave applications, and the development of low-loss lines for Terahertz frequency applications. She has also been theoretically and experimentally studying various types of uniplanar radiating structures for hybrid monolithic and monolithic oscillator and mixer designs.

Dr. Katehi is a member of the IEEE Antennas and Propagation Society, Microwave Theory and Techniques Society, Sigma Xi, Hybrid Microelectronics, URSI Commission D, and a member of IEEE Antennas and Propagation Society ADCOM from 1992 to 1995. She also serves as an Associate Editor for the IEEE TRANSACTIONS ON MICROWAVE THEORY TECHNIQUES. She was awarded the IEEE AP-S W. P. King Award in 1984, the IEEE AP-S S. A. Schelkunoff Award in 1985, the NSF Presidential Young Investigator Award (an URSI Young Scientist Fellowship) in 1987, the Humboldt Research Award in 1994, the University of Michigan Faculty Recognition Award in 1994, and the IEEE Microwave Theory and Techniques Society Microwave Prize in 1996.